Hindawi
Mathematical Problems in Engineering
Volume 2022, Article ID 6508811, 16 pages
https://doi.org/10.1155/2022/6508811

Research Article

Composite Terminal Guidance Law for Supercavitating Torpedoes with Impact Angle Constraints

Dongxue Xu, Jingyuan Zhang, Peng Wang, Xiaojia Yan, and Haidi Dong

College of Weapon Engineering, Naval University of Engineering, Wuhan 430033, China

Correspondence should be addressed to Peng Wang; yichen_wp@163.com

Received 22 September 2022; Revised 2 December 2022; Accepted 6 December 2022; Published 28 December 2022

Academic Editor: Xingling Shao

A novel composite terminal guidance law with impact angle constraints is proposed for supercavitating torpedoes to intercept maneuvering warships. Based on an adaptive super-twisting algorithm and nonsingular terminal sliding mode (NTSM), the proposed guidance law can guarantee the finite-time convergence of line-of-sight (LOS) angle error and the LOS angular rate error. The new guidance law is a combination of finite-time stability theory, sliding mode control (SMC), tracking differentiator (TD), disturbance observer (DO), and dynamic surface control. A high-order sliding mode TD is used for denoising, tracking, and differentiating the measured target heading angle. A novel DO, with its finite-time stability proved, is designed to estimate the target lateral acceleration for feedforward compensation to attenuate chattering in control input. In the case of a first-order-lag autopilot, a new kind of tracking differentiator is adopted to compute the first-order time derivative of the virtual control command, which can improve the accuracy of dynamic surface control and avoid the "explosion of items" problem encountered with the backstepping control. Finally, numerical simulation results are presented to validate the effectiveness and superiority of the proposed TD, DO, and the composite guidance law.

1. Introduction

It is generally assumed that supercavitating torpedoes (SCT) can only be designed for straight running, which may miss the target at the terminal phase. The latest researches indicate that a new kind of guidance based on the underwater electric field of target warships [1, 2] can be adopted to enhance SCT combat capability. By measuring the three components of the electric field, an SCT can obtain the target's location, velocity, and heading angle with a detection range of more than 1 km. The impact angle constraint refers to the interceptor attacking the target with a predetermined angle relative to the target's velocity vector. As for an SCT with a contact fuse, achieving a proper predetermined impact angle can ensure a high killing probability using the longitudinal length of the target warship. However, hitting the target with an impact angle constraint is challenging for traditional torpedoes and is especially difficult for SCT. Compared with traditional torpedoes, there are some new peculiarities of guided SCT: a significant increase in speed due to the supercavitation drag reduction effect, a smaller detection range due to the limitation of the detecting method, and limited maneuverability on account of cavity shape stabilization [3]. For the high-speed SCT with limited maneuverability attacking against the maneuvering target with impact angle constraint in a short time, traditional torpedo guidance laws are no longer suitable. New guidance laws for guided SCT have yet to be developed and deserve special attention.

Although there are no guidance laws with impact angle constraints for SCT in the public literature, an abundance of devotion has been made to study on high-speed interceptors, such as missiles and hypersonic aircraft. In recent years, guidance laws with impact angle constraints based on various fundamental theories have been proposed for different application scenarios. All the guidance laws can be classified into three main categories, i.e., modified proportional navigation (PN) guidance laws, modern guidance laws, and sliding mode control guidance laws.

Variations of PN were thoroughly studied for their simple structure, mature theory, and ease of implementation. In [4], a three-dimensional adaptive PN guidance approach is presented for a hypersonic vehicle to impact a stationary ground target with a specified direction in the terminal phase. In [5], a biased PN guidance law for passive homing missiles intercepting stationary targets with constrained impact angles is designed and analyzed. Ratnoo and Ghose [6] proposed an impact angle constrained PN guidance law against moving but non-maneuvering targets, with the navigation constant N being a function of the initial engagement geometry. In [7], a biased PN guidance law against maneuvering targets with impact angular constraint is proposed. The additional time-varying bias term compensates for target accelerations, sensor noises, and impact angle. The above guidance laws all assume that the maneuverability of the interceptor is much greater than that of the target, while SCT doesn't satisfy this assumption.

In [8], an optimal guidance law is presented for missiles with constant speed against stationary targets by adopting a time-to-go weighted energy cost function. However, accurately estimating the time-to-go is a tough challenge when the target is maneuvering and the interceptor's trajectory is highly curved. In [9], a linear-quadratic optimal-control-based guidance law and a linear-quadratic differential-game-based guidance law are derived, which enable imposing predetermined impact angles on maneuvering targets with significant initial heading errors. Closed-form solutions of optimal impact-angle-control guidance for a first-order lag system are derived in [10]. To reduce the complexity of the analytic solutions, ideal dynamics of the missiles are assumed, and an approximate time-to-go is used. However, the optimal-control-based and differential-game-based guidance laws are too complicated to derive and implement. Besides, they all rely on the accurate target motion model strictly, which cannot be obtained in practice.

Traditional SMC guidance laws can deal with the maneuvering target and dynamic uncertainties, yet they may lead to excessive or high-frequency chattering in control input. In [11], a guidance law with adaptive estimation for target maneuver is designed using two separate switching surfaces, one for regulating the impact angle constraints and the other for regulating the homing constraint. In [12], a kind of first-order sliding-mode guidance law with autopilot lag is proposed both for planar and three-dimensional interceptions in the presence of target maneuvers. In [13, 14], a hit-to-kill guidance strategy in the presence of target evasive maneuvers and dynamic uncertainty is developed based on the smooth second-order SMC.

In designing the guidance law for terminal interception, the general strategy is to nullify the relative velocity component perpendicular to the LOS [14]. This goal can be achieved by nulling the LOS rate for guidance laws without impact angle constraints. Nevertheless, when there is an impact angle constraint, it can only be achieved by nulling the LOS angle error and its first-order derivate, named the LOS angular rate error. In some literature, it is assumed that the final heading angle of the target can be acquired at the beginning [7] or that the desired LOS angle is fixed [15]. This assumption may be valid when the targets are nonmaneuvering but are improper when attacking maneuvering targets, and more details will be discussed in the subsequent section.

Another concern is that the terminal interception process is very short; thus, a finite-time convergence of the tracking errors is required. Finite-time convergence based on SMC consists of two parts, i.e., in the reaching phase, the sliding variable, which is a function of the tracking errors and their time derivatives, reaches zero or near zero in a short finite time; meanwhile, in the sliding phase, the tracking errors achieve finite-time convergence on the sliding surface. The terminal sliding mode control (TSMC), with the sliding variable as a nonlinear function of tracking errors, can improve the performance hugely. Guidance law with finite-time convergent impact angle based on TSMC for missiles has been proposed and studied in [16]. However, the TSMC does not prevail over the linear counterpart in the convergence rate when the system state is far from the equilibrium. Moreover, the TSMC suffers from a singularity problem, which will lead to control saturation. To get rid of the singularity, some new guidance laws are proposed to deal with non-maneuvering targets [17] and maneuvering targets [12, 18] based on nonsingular terminal sliding-mode control (NTSMC) [19]. A nonsingular fast terminal sliding mode control (NFTSMC) is introduced to achieve fast convergence performance, especially when the system states are far from equilibrium [20]. In [21], a nonlinear integral SMC method is employed for a finite-time stable strategy. On the other hand, different ways have been taken to regulate the switching surfaces for a finite reaching time, such as using adaptive sliding mode control [10], adopting the method of smooth second-order SMC [13, 14], and defining a switching control command [12, 15–18], which may cause the chattering phenomenon.

In addition, the guidance process requires real-time measurements of information such as LOS and target heading angle, which is inevitably contaminated by noise and can lead to large guidance deviations if unprocessed. Linear filters produce phase delays and amplitude distortions, whereas signal processing using a tracking differentiator (TD) can avoid these deficiencies. The TD-H proposed by Han [22] and rigorously proved by Guo and Zhao [23] has the advantage of minimum-time convergence and has been utilized in different fields, such as constructing a transient profile according to the actuator's capacity [24]. However, only estimates of the input and its first-order derivative can be obtained by TD-H. Several other kinds of TDs, which have the merits of simple recursive structure, easily adjusting parameters, and high accuracy, have been proposed by Levant [25–27]. Nevertheless, these TDs, both the conventional version [25, 26] and its improved version (TD-L) [27], all suffer from significant undesirable overshoot during the transient. Recently, a new high-order adaptive sliding mode TD was presented (TD-N) [28], which adaptively changes its gains for improved tracking performances and reduced overshoot.

An interceptor's autopilot lag can significantly influence guidance accuracy, especially in the presence of target maneuvers [12]. In some literature, the autopilot dynamic is

treated as ideal, introducing significant control biases [29]. The traditional design methodology for handling autopilot lag is the backstepping control, which may lead to the "explosion of items" problem. The dynamic surface control proposed by Swaroop et al. [30] can avoid this problem by calculating the time derivative of the virtual control command through the first-order filter, which is a standard method for dealing with similar issues at present [31, 32]. However, it will inevitably induce a phase delay, which reduces convergence speed and control precision.

In guidance design, the lateral acceleration of the target can be regarded as an unknown bounded disturbance, which can be estimated by using a disturbance observer and cancelled by feedforward compensation simultaneously. As a result, the chattering caused by excessive switching control can be mitigated. In [13, 15, 16] and [21], sliding mode disturbance observers are used to estimate target lateral acceleration. In [31, 33], extended state observers (ESO) are used for the same purpose. The inherent drawbacks of these observers are that they are prone to overshoot during the transition period and do not work well under noise conditions.

A novel composite guidance law is proposed to address the problems aforementioned in existing guidance laws. Under the novel guidance law, an SCT can hit a maneuvering warship target with an impact angle constraint. Compared with the existing methods, the main highlights of the proposed solution are outlined as follows:

(1) In the guidance law design, the second-order time derivative of the target heading angle is needed, which is usually regarded as zero in the present literature, for it is hard to get. A recently proposed high-order sliding mode TD [27], which performs well in handling noisy signals, is used to track the measured noisy target heading angle and obtain its second-order time derivative.

(2) A novel high-order sliding mode DO is designed based on TD [27], and its finite-time stability is proved using homogeneous theory. The novel DO is applied to estimate the target lateral acceleration, which is regarded as an unknown disturbance.

(3) A new fast nonsingular terminal sliding manifold is designed, and an adaptive super-twisting algorithm is applied, both of which help to lower the control input of autopilot at the initial time. The finite-time convergence analysis of the tracking errors is carried out by Lyapunov theory under a novel framework.

(4) To effectively account for the autopilot lag of the SCT, the variable gain sliding mode TD [27] is used to calculate the first-order time derivative of the virtual control command, which improves the tracking accuracy and avoids the "explosion of items" problem at the same time.

The rest of this paper is arranged as follows. In Section 2, the engagement dynamics are derived. In Section 3, a new sliding mode tracking differentiator is introduced, and a novel sliding mode disturbance observer is designed. In Section 4, the nonsingular terminal sliding manifold and an adaptive second-order SMC algorithm are designed. In Section 5, numerical simulations are carried out for performance evaluations of new TD, DO, and the proposed composite guidance law. Finally, in Section 6, some conclusions and discussions are offered.

2. Problem Formulation

The planar engagement and the relative motion dynamics are derived based on the vector derivative algorithm rather than differentiating equations [15]. The relationship between the impact angle and the LOS angle is derived, and the mistake in treating the desired LOS angle as a fixed value in the existing literature is analyzed.

To simplify the analysis of the pursuer-target relative motion, the interception is assumed to occur in a planar engagement scenario, with the target and torpedo treated as point masses, and denoted by T and M, respectively.

In the LOS coordinate system as shown in Figure 1, the origin is fixed at the torpedo, r represents the relative range of torpedo-to-target, θ_M and θ_T are the heading angles of the torpedo and the target, and q is the LOS angle. Moreover, V_M and V_T, respectively, denote the velocities of the torpedo and the target, both of which are assumed to be constant. The a_M and a_T, respectively, refer to the accelerations of the torpedo and the target, which are perpendicular to their velocity directions. Let $\eta_M = q - \theta_M$, and $\eta_T = q - \theta_T$, and then, we have $\dot{\theta}_T = a_T/V_T$, and $\dot{\theta}_M = a_M/V_M$ [16].

In the coordinate system, subscripts r and q represent the radial direction along the LOS and the axial direction normal to the LOS. The base vector along the LOS is denoted by $\mathbf{e}_r$, while the one normal to the LOS is aligned with $\mathbf{e}_r$ rotating $\pi/2$ counter-clockwise, denoted by $\mathbf{e}_q$.

The derivatives of the base vectors are

$$\frac{d}{dt}\begin{bmatrix}\mathbf{e}_r\\ \mathbf{e}_q\end{bmatrix} = \begin{bmatrix}0 & \dot{q}\\ -\dot{q} & 0\end{bmatrix}\begin{bmatrix}\mathbf{e}_r\\ \mathbf{e}_q\end{bmatrix}, \tag{1}$$

where $\dot{q}$ refers to the LOS angular rate. It is evident from (1) that the velocity vector is

$$\begin{aligned}\mathbf{v} &= \frac{\mathrm{d}\mathbf{r}}{\mathrm{d}t}\\ &= \frac{\mathrm{d}(r\mathbf{e}_r)}{\mathrm{d}t}\\ &= \frac{\mathrm{d}r}{\mathrm{d}t}\mathbf{e}_r + r\frac{\mathrm{d}\mathbf{e}_r}{\mathrm{d}t}\\ &= \dot{r}\mathbf{e}_r + r\dot{q}\mathbf{e}_q.\end{aligned} \tag{2}$$

Defining V_r as the relative velocity between torpedo and target along the LOS, and V_q as the one normal to the LOS, (2) can be rewritten as follows:

$$\begin{cases} V_r = V_{Tr} - V_{Mr} = -V_M\cos\eta_M + V_T\cos\eta_T = \dot{r},\\ V_q = V_{Tq} - V_{Mq} = V_M\sin\eta_M - V_T\sin\eta_T = r\dot{q}.\end{cases} \tag{3}$$

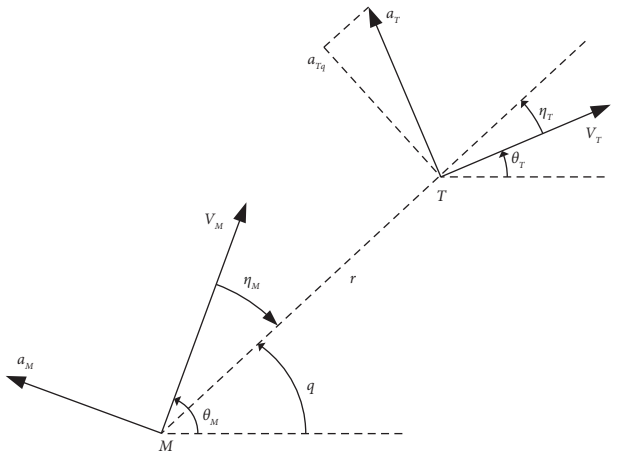

Figure 1: Planar torpedo-target engagement.

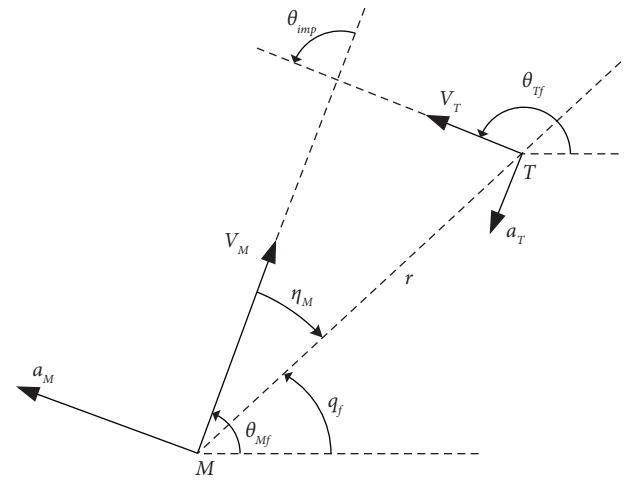

Figure 2: The interception triangle.

Identically, differentiating (2) with respect to time yields

$$\begin{aligned}\mathbf{a} &= \frac{\mathrm{d}\left(\dot{r}\mathbf{e}_r + r\dot{q}\mathbf{e}_q\right)}{\mathrm{d}t} \\ &= \frac{\mathrm{d}\dot{r}}{\mathrm{d}t}\mathbf{e}_r + \dot{r}\frac{\mathrm{d}\mathbf{e}_r}{\mathrm{d}t} + \frac{\mathrm{d}r}{\mathrm{d}t}\dot{q}\mathbf{e}_q + r\left(\frac{\mathrm{d}\dot{q}}{\mathrm{d}t}\mathbf{e}_q + \frac{\mathrm{d}\mathbf{e}_q}{\mathrm{d}t}\dot{q}\right) \\ &= \left(\ddot{r} - r\dot{q}^2\right)\mathbf{e}_r + (r\ddot{q} + 2\dot{r}\dot{q})\mathbf{e}_q.\end{aligned} \tag{4}$$

Similarly, defining a_r as the relative acceleration of the torpedo target along the LOS, and a_q as the one normal to the LOS, (4) can be rewritten as follows:

$$\left\{a_r = a_{Tr} - a_{Mr} = a_T \sin\eta_T - a_M \sin\eta_M = \ddot{r} - r\dot{q}^2, a_q = a_{Tq} - a_{Mq} = a_T \cos\eta_T - a_M \cos\eta_M = r\ddot{q} + 2\dot{r}\dot{q}.\right. \tag{5}$$

With a transposition, (5) can be transformed to

$$\begin{cases}\ddot{r} = r\dot{q}^2 - a_{Mr} + a_{Tr}, \\ r\ddot{q} = -2\dot{r}\dot{q} + a_{Tq} - a_{Mq}.\end{cases} \tag{6}$$

Combining (3) and (6), one can imply that

$$\begin{aligned}\dot{V}_q &= r\ddot{q} + \dot{r}\dot{q} \\ &= -\dot{r}\dot{q} + a_{Tq} - a_{Mq}.\end{aligned} \tag{7}$$

The autopilot can be approximately described by the following first-order dynamics [12, 15]:

$$\dot{a}_M = -\frac{a_M}{\tau} + \frac{u}{\tau}, \tag{8}$$

where τ is the autopilot lag, and u is the acceleration command for the autopilot.

As shown in Figure 2, the impact angle is described as the angle between the velocity vectors of the torpedo and the target at the time of interception [18], i.e.,

$$\theta_{\mathrm{imp}} = \theta_T - \theta_{Mf}. \tag{9}$$

The relative velocity component should be nullified to form a collision triangle [6, 7].

$$\begin{cases}V_{qf} = r_f\dot{q}_f = 0, \\ V_M \sin\left(\theta_{Mf} - q_f\right) = V_T \sin\left(\theta_T - q_f\right).\end{cases} \tag{10}$$

With (9) and the trigonometric equation in (10), the relationship between the desired LOS angle and the impact angle [6, 11] can be derived as follows:

$$q_f = \theta_T - \arctan\left(\frac{\sin\theta_{\mathrm{imp}}}{\cos\theta_{\mathrm{imp}} - \nu_1}\right), \tag{11}$$

where the target-to-torpedo velocity ratio is $\nu_1 = V_T/V_M < 1$.

It is evident that q_f and θ_T are linear with only one constant bias. For a maneuvering target, θ_T is a time-varying quantity, and so is the q_f. In practice, the terminal heading angle of the maneuvering target is generally unavailable at the beginning of guidance, implying that the q_f cannot be treated as a given constant as in [15]. In other words, it is impossible to regulate the $\dot{q}$ at near zero while keep the q tracking a varying desired q_f simultaneously. Furthermore, with θ_{imp} and ν_1 predetermined, on differentiating (11), one can imply that

$$\begin{cases} \dot{q}_f = \dot{\theta}_T = \dfrac{a_T}{V_T} = \dfrac{a_{Tq}}{V_T \cos \eta_T}, \\ \ddot{q}_f = \ddot{\theta}_T = \dfrac{\dot{a}_T}{V_T} = \dfrac{\dot{a}_{Tq} + a_{Tq}\dot{\eta}_T \tan \eta_T}{V_T \cos \eta_T}. \end{cases} \tag{12}$$

It can be seen from the above analysis that, to achieve the impact angle constraints, the first-order and second-order time derivatives of the target heading angle, $\dot{\theta}_T$ and $\ddot{\theta}_T$, are needed. Or else, the target lateral acceleration a_{Tq} as well as its first-order time derivative $\dot{a}_{Tq}$ are required. In the present literature, $\ddot{\theta}_T$ or $\dot{a}_{Tq}$ is usually regarded as zero because they are hard to get. Here, two equivalent solutions are proposed to deal with this problem. The first method is to get the $\dot{\theta}_T$ and $\ddot{\theta}_T$ using a second-order TD, and the other way is to estimate the a_{Tq} and $\dot{a}_{Tq}$ based on a third-order DO. Here, the first method is adopted in this paper.

Let $x_1 = q - q_f$, $x_2 = \dot{q} - \dot{q}_f$, and $x_3 = a_M$. It follows from (6), (8), and (12) that

$$\begin{cases} \dot{x}_1 = x_2, \\ \dot{x}_2 = -\dfrac{2\dot{r}\dot{q}}{r} - x_3 \cdot \dfrac{\cos \eta_M}{r} + \dfrac{a_{Tq}}{r} - \ddot{\theta}_T, \\ \dot{x}_3 = -\dfrac{x_3}{\tau} + \dfrac{u}{\tau}. \end{cases} \tag{13}$$

In designing a guidance law with an impact angle constraint, the unknown external disturbance includes the target lateral acceleration a_{Tq}, as well as the second-order time derivative of the target heading angle $\ddot{\theta}_T$. The design objective of control input u is to drive x_1 and x_2 to zero in finite time, that is, $q \longrightarrow q_f$, $\dot{q} \longrightarrow \dot{q}_f$.

3. High-Order Sliding Mode Tracking Differentiator and Design of New Disturbance Observer

In this section, a high-order sliding mode TD for processing measurement signals with noise is introduced. A new kind of sliding mode DO adapted from the high-order sliding mode TD is designed, and the finite-time stability of the proposed DO is proved using homogeneous degree theory.

Firstly, some conclusions are recalled, which are indispensable in subsequent analysis.

3.1. Essential Preliminary Concepts

Lemma 1 (see [34]). *Define a smooth vector field*

$$f(x_1, \cdots, x_n) = [f_1(x), \cdots, f_n(x)]^T : \mathbb{R}^n \longrightarrow \mathbb{R}^n, \tag{14}$$

and the dilation

$$\Delta_\eta = (r_1, \cdots, r_n) \in \mathbb{R}^n, \tag{15}$$

where $x_1, \cdots, x_n$ are suitable coordinates on $\mathbb{R}^n$ and $r_1, \cdots, r_n$ are positive real numbers. The vector field (14) is homogeneous of degree $m \in R$, if $\forall \eta > 0$, $i = 1, 2, \cdots, n$, f_i is a homogeneous function with respect to dilation (15)

$$f_i(\eta^{r_1} x_1, \cdots, \eta^{r_n} x_n) = \eta^{r_i + m} f_i(x_1, \cdots, x_n). \tag{16}$$

Suppose the origin is a stable equilibrium of $f(x)$, if its degree of homogeneity, $m \geqslant -\max\{r_i\}$, is negative, then the origin is finite-time stable.

Lemma 2 (see [15]). *Finite-time convergence theory.*

On system $\dot{x} = f(x, t)$, $f(0, t) = 0$, $x \in \mathbb{R}^n$, suppose $f: U_0 \times R \longrightarrow \mathbb{R}^n$ is a C^1 smooth, positive definite function on $U \subset \mathbb{R}^n$ and $\dot{V}(x) + \beta_1 V^{\beta_2}(x)$ is a negative semidefinite function on $U \subset \mathbb{R}^n$, where $\beta_1 > 0$ and $\beta_2 \in (0, 1)$, then there exists an area $U_0 \subset \mathbb{R}^n$ such that $V(x)$ starting from $U_0 \subset \mathbb{R}^n$ can reach $V(x) \equiv 0$ in finite time

$$T_{\text{reach}} \leqslant \frac{V^{1-\beta_2}(x_0)}{[\beta_1 (1 - \beta_2)]}. \tag{17}$$

3.2. Tracking Differentiator for Processing Measured Target Heading Angle

Lemma 3 (see [35]). *Suppose the unknown function $f_0(t)$, $t \geq 0$, has a noisy approximation $f(t) = f_0(t) + n(t) + n_c(t)$ available in real time, where the derivative $f_0^{(k)}(t)$ exists, and there is a known Lipschitz constant $L > 0$. The first noise term $n(t)$ is Lebesgue-measurable and bounded by $\exists \delta > 0$, $|n(t)| < \delta$, and the second noise term $n_c(t)$ is integrable.*

The kth-order tracking differentiator proposed is

$$\begin{cases} \dot{w}_{-1} = -\lambda_{k+1} L^{1/k+2} \left| w_{-1} \right|^{k+1/k+2} \text{sign}(w_{-1}) + w_0 - f(t), \\ \dot{w}_0 = -\lambda_k L^{2/k+2} \left| w_{-1} \right|^{k/k+1} \text{sign}(w_{-1}) + w_{1,} \\ \vdots, \\ \dot{w}_{k-1} = -\lambda_1 L^{k+1/k+2} \left| w_{-1} \right|^{1/k+1} \text{sign}(w_{-1}) + w_k, \\ \dot{w}_k = -\lambda_0 L \left| w_{-1} \right|^{0} \text{sign}(w_{-1}), \end{cases} \tag{18}$$

where $\text{sign}(\cdot)$ is signum function. $\lambda_i > 0$, $i = 0, 1, \cdots, k+1$, as well as the design parameter L can be set follows [25]. Moreover, w_{-1} is an auxiliary variable, while w_i, $i = 0, 1, \cdots, k$, is the estimate of $f_0^{(i)}(t)$, with the estimation errors converging in finite time. Increasing L contributes to the convergence rate, but it also degrades the noise-attenuating performance, so there is a trade-off between the convergence rate and the convergence precision.

A second-order TD for processing noisy measured target heading angle, denoted by $\widetilde{\theta}_T$, is designed with Lemma 2 using TD (18):

$$\begin{cases} \dot{w}_{-1} = -\lambda_{13} L_1^{1/4} \left| w_{-1} \right|^{3/4} \operatorname{sign}\left(w_{-1}\right) + w_0 - \widetilde{\theta}_T, \\ \dot{w}_0 = -\lambda_{12} L_1^{2/4} \left| w_{-1} \right|^{2/4} \operatorname{sign}\left(w_{-1}\right) + w_1, \\ \dot{w}_1 = -\lambda_{11} L_1^{3/4} \left| w_{-1} \right|^{1/4} \operatorname{sign}\left(w_{-1}\right) + w_2, \\ \dot{w}_2 = -\lambda_{10} L_1 \left| w_{-1} \right|^{0} \operatorname{sign}\left(w_{-1}\right). \end{cases} \tag{19}$$

With the proper parameters selected, we have

$$\begin{gathered} w_0 = \widehat{\theta}_T, \\ w_1 = \dot{\widehat{\theta}}_T, w_2 = \ddot{\widehat{\theta}}_T. \end{gathered} \tag{20}$$

3.3. Proposal of New Disturbance Observer and Its Application in Estimating Target Lateral Acceleration. Consider the following first-order SISO dynamics:

$$\dot{x} = u_1 + d, \tag{21}$$

where x is the system state, u_1 is the control input and is Lebesgue-measurable, and d is the lumped disturbance and is sufficiently smooth. Adapted from TD (18), the proposed DO is

$$\begin{cases} \dot{z}_{-1} = -\lambda_{k+1} L^{1/k+2} \left| z_{-1} \right|^{k+1/k+2} \operatorname{sign}\left(z_{-1}\right) + z_0 - x, \\ \dot{z}_0 = -\lambda_k L^{2/k+2} \left| z_{-1} \right|^{k/k+2} \operatorname{sign}\left(z_{-1}\right) + z_1 + u_1, \\ \quad \vdots \\ \dot{z}_{k-1} = -\lambda_{k-i} L^{k+1/k+2} \left| z_{-1} \right|^{1/k+2} \operatorname{sign}\left(z_{-1}\right) + z_k, \\ \dot{z}_k = -\lambda_0 L \left| z_{-1} \right|^{0} \operatorname{sign}\left(z_{-1}\right), \end{cases} \tag{22}$$

where $\lambda_i > 0, i = 0, 1, \cdots, k+1$, $L > |d^{(k)}|$.The z_{-1} is an auxiliary variable, while z_0 is the estimate of x, z_i is the estimate of $d^{(i-1)}$, $i = 1, \cdots, k$, i.e.,

$$\begin{gathered} z_0 = \widehat{x}, \\ z_1 = \widehat{d}, \cdots, \\ z_k = \widehat{d}^{(k-1)}. \end{gathered} \tag{23}$$

Theorem 1. *The estimation errors of (22) converge in finite time.*

Proof. Here, we denote

$$\begin{cases} \sigma_{-1} = \dfrac{z_{-1}}{L}, \sigma_0 = \dfrac{\left(z_0 - x\right)}{L}, \\ \sigma_i = \dfrac{\left[z_i - d^{(i-1)}\right]}{L}, i = 1, 2, \cdots, k. \end{cases} \tag{24}$$

Using (22) and (24) and $d^{(k)}/L \in [-1, 1]$, any solution of (22) is governed by the following differential inclusion in the Filippov sense:

$$\begin{cases} \dot{\sigma}_{-1} = -\lambda_{k+1} \left| \sigma_{-1} \right|^{k+1/k+2} \operatorname{sign}\left(\sigma_{-1}\right) + \sigma_0, \\ \dot{\sigma}_0 = -\lambda_k \left| \sigma_{-1} \right|^{k/k+2} \operatorname{sign}\left(\sigma_{-1}\right) + \sigma_1, \\ \quad \vdots, \\ \dot{\sigma}_i = -\lambda_{k-i} \left| \sigma_{-1} \right|^{k-i/k+2} \operatorname{sign}\left(\sigma_{-1}\right) + \sigma_{i+1}, i = 1, 2, \cdots, k-1, \\ \quad \vdots, \\ \dot{\sigma}_k = -\lambda_0 \operatorname{sign}\left(\sigma_{-1}\right) - d^{(k)}/L \in -\lambda_0 \operatorname{sign}\left(\sigma_{-1}\right) + [-1, 1]. \end{cases} \tag{25}$$

Introduce the vector field g: $\mathbb{R}^{k+2} \longrightarrow \mathbb{R}^{k+2}$

$$\begin{aligned} g\left(\sigma_{-1}, \cdots, \sigma_k\right) &= \left[g_1, \cdots, g_j \cdots, g_{k+2}\right]^T \\ &= \left[\dot{\sigma}_{-1}, \cdots, \dot{\sigma}_{j-2}, \cdots, \dot{\sigma}_k\right]^T, \end{aligned} \tag{26}$$

where $j = 2, \cdots, k+1$. The trajectories of function (26) are invariant concerning the transformation [36]

$$\forall \eta > 0, G_\eta\colon \ \left(t, \sigma_i\right) \longmapsto \left(\eta t, \eta^{k-i+1} \sigma_i\right), i = -1, 0, 1, \cdots, k. \tag{27}$$

By combining (25)–(27), one can imply that

$$\begin{cases} g_j\left(\eta t, \eta^{k+2} \sigma_{-1}, \eta^{k-j+3} \sigma_{j-2}, \eta^{k-j+2} \sigma_{j-1}\right) = \eta^{(k-j+3)+(-1)} g_j\left(t, \sigma_{-1}, \sigma_{j-2}, \sigma_{j-1}\right), \\ g_{k+2}\left(\eta t, \eta^{k+2} \sigma_{-1}, \eta \sigma_k\right) = \eta^{1+(-1)} g_{k+2}\left(t, \sigma_{-1}, \sigma_k\right). \end{cases} \tag{28}$$

One can note that the differential inclusion (25) is homogeneous of degree -1 with respect to dilation $(k+2, \cdots, k-j+3, \cdots, 1)$, $j = 2, \cdots, k+1$; therefore, it is finite-time stable by Lemma 1.

External disturbance increases the chattering in autopilot control input, yet it can be mitigated by feedforward compensation. With total disturbance compensated, the guidance law can be designed in the nominal system according to the required control accuracy. A new DO is constructed to estimate the a_{Tq} based on (7) using DO (22):

$$\begin{cases} \dot{z}_{-1} = -\lambda_{22} L_2^{1/3} \left| z_{-1} \right|^{2/3} \operatorname{sign}\left(z_{-1}\right) + z_0 - r\dot{q}, \\ \dot{z}_0 = -\lambda_{21} L_2^{2/3} \left| z_{-1} \right|^{1/3} \operatorname{sign}\left(z_{-1}\right) + z_1 - \dot{r}\dot{q} - a_M \cos \eta_M, \\ \dot{z}_1 = -\lambda_{20} L_2 \left| z_{-1} \right|^{0} \operatorname{sign}\left(z_{-1}\right). \end{cases} \tag{29}$$

With a proper choice of the parameters L_2 and λ_{2i}, $i = 0, 1, 2$, z_1 approaches to a_{Tq} in a short, finite time. It should be noted that, in some literature, the DO for estimating a_{Tq} is based on (6), with the item a_{Tq}/r estimated. However, in this

way, extensive tracking range is to be handled for a_{Tq}/r change with r dramatically as the torpedo approaches the target, and difficulties will be encountered in choosing parameters [37]. In addition, the proposed disturbance observer can also be utilized in other scenarios such as control of quadrotors [38].

4. Composite Sliding Mode Guidance Law with Finite-Time Convergence

Firstly, a new nonsingular terminal sliding manifold (NNTSM) is designed. Then, an adaptive super-twisting algorithm (ASTA) to deal with the unknown upper bounded disturbance is designed. Finally, using the variable gain sliding mode tracking differentiator (TD-N), the control input for autopilot with a first-order dynamic is obtained.

The TD (19) designed for processing noisy target heading angle is referred to as TD1. The DO (29) designed for estimating the target lateral acceleration is referred to as DO1. The structure of the guidance law is shown in Figure 3.

4.1. Design of Virtual Control Input Based on NNTSM and ASTA. Traditional TSM can only guarantee asymptotical convergence rather than finite-time convergence. Inspired by [20, 34] and [39], a new nonsingular terminal sliding mode control is introduced to improve the convergence rate, with its sliding manifold designed as follows:

$$s = x_2 + \sum_{1=1}^{2} \int_0^t c_i\left(1 - e^{-t/\tau_i}\right)\left|x_i\right|^{\alpha_i} \operatorname{sign}(x_i) \bullet \mathrm{d}t, \tag{30}$$

where $\alpha_2 \in (0,1)$, $\alpha_1 = \alpha_2/(2-\alpha_2) \in (0,1)$, c_1, c_2 ensure that $l^2 + c_2 l + c_1 = 0$ is Hurwitz, and their choices can be referred to [39]. In addition, $\tau_1 = \tau_2 > 0$ and can be set by trial and error considering the torpedo's maneuverability limit and the reaching time.

A main drawback in the standard super-twisting algorithm is that the upper bounds of disturbance and its first-order time derivative are needed in choosing parameters. Inspired by [40, 41], an adaptive super-twisting algorithm (ASTA) is designed as follows:

$$\begin{cases} \dot{s} = -k_1 \phi_1 - \int_0^t \mathrm{d}t + d, \\ \phi_1 = |s|^{1/2} \operatorname{sign}(s), \phi_2 = \dfrac{1}{2} \operatorname{sign}(s), \end{cases} \tag{31}$$

where k_1 and k_2 are adaptive gains with the nonlinear adaptation law as follows [41]:

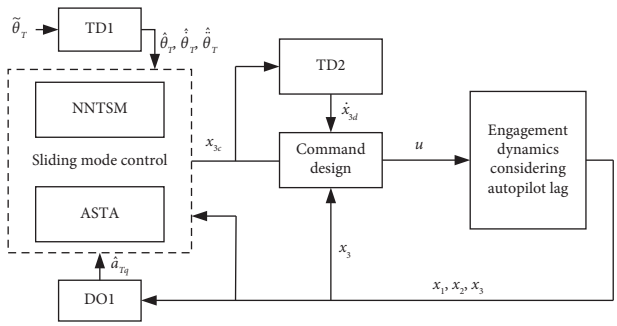

Figure 3: Structure flowchart of compound guidance law.

$$\dot{k}_1 = \begin{cases} \gamma|s|, & k_1 \le k_m, \\ \lambda\sqrt{|s|}\,\operatorname{sign}(|s| - \varepsilon), & k_1 > k_m, \end{cases}, k_1(0) > 0, k_2 = 2\delta k_1, \tag{32}$$

where γ, λ, ε, k_m, and δ are all positive constants.

A small ε can improve the controller accuracy, but it will also reduce the convergence rate of s [42]. Increasing the control parameters λ, γ, and δ can shorten the convergence time and increase the control accuracy, but it also augments the acceleration magnitude. Thus, there is a trade-off needed in tuning parameters.

Proposition 1. *Given the sliding variable dynamics (31) and the gain-adaptation law (32), the gains k_1 and k_2 are upper bound, i.e., there exists $k_1^* > 0$ and k_2^* such that*

$$\begin{cases} \tilde{k}_1 = k_1 - k_1^* \le 0, \\ \tilde{k}_2 = k_2 - k_2^* \le 0. \end{cases} \tag{33}$$

Sketch Proof of Proposition 1. Since there is a positive linear correlation between k_1 and k_2, only k_1 is analyzed for clarity.

If the sliding variable $|s| > \varepsilon$, k_1 and k_2 increases gradually enough to make the sliding variable s converge to zero. Once the sliding mode is established, i.e., $|s| < \varepsilon$, the proposed gain-adaptation law (32) will keep k_1 approaching k_m. If gains are not large enough to counteract the perturbations, resulting in $|s| > \varepsilon$, k_1 will increase again making the sliding variable converge to $|s| < \varepsilon$. Therefore, adaptive parameters are always globally bounded, and a detailed proof can be referred to [42].

Taking (13), (30) and (31) into account, the virtual control command can be chosen as

$$x_{3c} = \frac{r}{\cos\eta_M}\left[\sum_{i=1}^{2} c_i\left(1 - e^{-t/\tau_i}\right)\left|x_i\right|^{\alpha_i} \operatorname{sign}(x_i) - \hat{\theta}_T - \frac{2\dot{r}\dot{q}}{r} + \frac{\hat{a}_{Tq}}{r} + k_1\phi_1 + \int k_2\phi_2 \mathrm{d}t\right]. \tag{34}$$

The prominent merits of the sliding manifold (30) and the ASTA can be inferred from the virtual control command (34). In the reaching phase, x_{3c} is attenuated with $1 - e^{-t/\tau_i} < 1$; wheras in the sliding phase there is $t > t_r$, with

$c_i(1-e^{-t/\tau_i})$ approaching to c_i, the convergence rate on the sliding surface will not be affected. In addition, adaptive gains k_1 and k_2 are gradually increasing, reducing x_{3c} at the start of guidance.

4.2. Design of Autopilot Control Input via New Tracking Differentiator. Considering the autopilot lag, dynamic surface control [30] is frequently used to design the control input. From (13), the theoretical command input for the autopilot should be

$$u = \tau\dot{x}_{3c} + x_{3c}. \tag{35}$$

One significant difficulty in calculating u is to get the first-order time derivative of x_{3c}. In dynamic surface control, x_{3c} is passed through a first-order filter, getting x_{3d} and $\dot{x}_{3d}$, and the "explosion of items" problem in the backstepping control is avoided. Nevertheless, the use of a low-pass filter may introduce a significant delay as well as a magnitude attenuation. Thus x_{3c} is not followed precisely by x_{3d}. Even more, in the dynamic surface method, with the accuracy of $\dot{x}_{3c} - \dot{x}_{3d}$ not guaranteed, the controller can only be designed to regulate x_3 tracking x_{3d}. Though the error between x_3 and x_{3d} can be removed by feedback control, there is still an error between x_3 and x_{3c}, resulting in reduced tracking accuracy. In some literature, TD proposed by Han [22] is used to replace the low-pass filter, yet it may lead to a phase lag in the transient period. In this paper, x_{3c} is passed through an improved sliding mode TD [28], getting new x_{3d} and $\dot{x}_{3d}$. The improved TD has slighter overshoot and faster response speed, which can guarantee the accuracy of $\dot{x}_{3c} - \dot{x}_{3d}$. Then feedback control is carried out to improve the control accuracy of $x_3 - x_{3c}$. In this way, improved control accuracy is achieved, while the common "explosion of items" problem in the backstepping control design is avoided.

The TD2 for dealing with x_{3c} can be constructed as

$$\begin{cases} c(t) = \dfrac{\kappa\left(\max\limits_{z\in[t-\tau_0,t]}\{m_0(z)\} - \min\limits_{z\in[t-\tau_0,t]}\{m_0(z)\}\right)}{(t-\tau_0)}, \\ L_3(t) = \chi\left|m_{-1}(t)\right| + c(t), \\ v(t) = -\lambda_{32}L_3^{1/3}(t)\left|m_{-1}(t)\right|^{2/3}\operatorname{sign}\left[m_{-1}(t)\right] + m_0(t) - x_{3c}(t), \\ \dot{m}_{-1}(t) = v(t) - \beta|v(t)|\operatorname{sign}\left[m_{-1}(t)\right], \\ \dot{m}_0(t) = -\lambda_{31}L_3^{2/3}(t)\left|m_{-1}(t)\right|^{1/3}\operatorname{sign}\left[m_{-1}(t)\right] + m_1(t), \\ \dot{m}_1(t) = -\lambda_{30}L_3(t)\left|m_{-1}(t)\right|^{0}\operatorname{sign}\left[m_{-1}(t)\right], \end{cases} \tag{36}$$

where $\lambda_{3i} > 0$, $i = 0, 1, 2$, and can be set following [27]. The c reflects the average change rate of the input, while v and m_{-1} are auxiliary variables. $m_0 = x_{3d}$, $m_1 = \dot{x}_{3d}$ are the estimates of x_{3c} and $\dot{x}_{3c}$, respectively. Moreover, $\chi > 0$, $\kappa > 0$, $0 \le \beta < 1$, and $\tau_0 > 0$. Increasing χ contributes to the tracking response speed but will also increase the overshoot magnitude in the transient phase. A big β can reduce overshoot, but it also restrains response speed at the same time. Increase of κ can improve tracking speed and reduce overshoot, but it can also augment the effect of noise. The stability proof and parameter selection rules of the variable gain sliding mode TD are presented in [28].

The actual command input for the autopilot is

$$u = \tau\dot{x}_{3d} + x_{3c}. \tag{37}$$

Denote the error $y_3 = x_3 - x_{3c}$, and then substitute (13) and (34) into (37) yields

$$\begin{aligned} \dot{y}_3 &= \dot{x}_3 - \dot{x}_{3c} \\ &= -\frac{y_3}{\tau} + \dot{x}_{3d} - \dot{x}_{3c}. \end{aligned} \tag{38}$$

With the proven finite-time convergence of the DO1, TD1, and TD2, there must exist small $\varepsilon_1, \varepsilon_2, \varepsilon_3 > 0$ such that

$$\begin{aligned} &\left|\widehat{a}_{Tq} - a_{Tq}\right| < \varepsilon_1, \\ &\left|\hat{\ddot{\theta}}_T - \ddot{\theta}_T\right| < \varepsilon_2, \left|\dot{x}_{3c} - \dot{x}_{3d}\right| < \varepsilon_3. \end{aligned} \tag{39}$$

Since $\dot{y}_3 < -y_3/\tau + \varepsilon_3$, τ is small, it follows that the tracking error y_3 is ultimately uniformly.

Confined by ε_3. Thus x_3 can track the virtual control command x_{3c} precisely.

Substituting (13) and (34) into (30) yields

$$\begin{aligned} \dot{s} &= \dot{x}_2 + \sum_{i=1}^{2} c_i\left(1-e^{-t/\tau_i}\right)\left|x_i\right|^{\alpha_i}\operatorname{sign}(x_i) \\ &= -\frac{2\dot{r}\dot{q}}{r} - \frac{(x_{3c}+y_3)\cos\eta_M}{r} + \frac{a_{Tq}}{r} - \ddot{\theta}_T + \sum_{i=1}^{2} c_i\left(1-e^{-t/\tau_i}\right)\left|x_i\right|^{\alpha_i}\operatorname{sign}(x_i) \\ &= -k_1\phi_1 - \int k_2\phi_2 \mathrm{d}t + d, \end{aligned} \tag{40}$$

where the lumped disturbance

$$d = \frac{a_{Tq} - \widehat{a}_{Tq}}{r} + \hat{\ddot{\theta}}_T - \ddot{\theta}_T - \frac{\cos\eta_M}{r}y_3. \tag{41}$$

According to (38) and (39), d should be bounded.

4.3. Finite-Time Convergence Analysis of the Tracking Errors

Theorem 2. *The tracking errors of the LOS angle x_1 and LOS angular rate x_2 will converge into a small region near zero in finite time.*

The proof can be divided into two steps. Firstly, we prove that the sliding variable s will converge into a neighbourhood $\Omega_0 = \{s \| |s| < \varepsilon\}$ in finite time under the control of the adaptive super-twisting algorithm (32). Secondly, we prove that the tracking errors are finite-time convergent on the sliding surface.

Inspired by [43, 44], a novel proof of this theorem under a new framework is proposed, which can be regarded as a modified version of the proof in [41].

To facilitate the stability analysis, a new state vector is introduced:

$$\begin{aligned}\boldsymbol{\xi}^T &= [\xi_1, \xi_2]^T \\ &= \left[\phi_1, -\int k_2\phi_2 \mathrm{d}t + d\right]^T,\end{aligned} \tag{42}$$

then combining (31) and (40) into

$$\begin{cases} \dot{s} = -k_1\phi_1 + \xi_2, \\ \dot{\xi}_2 = -k_2\phi_2 + \dot{d}. \end{cases} \tag{43}$$

System (42) can be rearranged as

$$\begin{aligned}\dot{\boldsymbol{\xi}} &= \left[\dot{\phi}_1\left(-k_1\phi_1 - \int k_2\phi_2 \mathrm{d}t + d\right) - k_2\phi_2 + \dot{d}\right] \\ &= \dot{\phi}_1\left[\left(-k_1\phi_1 - \int k_2\phi_2 \mathrm{d}t + d\right) - k_2\phi_1 + \frac{\dot{d}}{\dot{\phi}_1}\right] \\ &= \dot{\phi}_1\left[\mathbf{A}\boldsymbol{\xi} + \mathbf{B}\tilde{g}\right],\end{aligned} \tag{44}$$

where $\dot{\phi}_1 = \mathrm{d}\phi_1/\mathrm{d}s = |s|^{-1/2}/2 = \phi_2/\phi_1$, $\tilde{g} = \dot{d}/\dot{\phi}_1 = 2\dot{d}|\phi_1|$, $\mathbf{B} = \begin{bmatrix} 0 & 1 \end{bmatrix}^T$, and

$$\mathbf{A} = \begin{bmatrix} -k_1 & 1 \\ -k_2 & 0 \end{bmatrix}. \tag{45}$$

Suppose there exists a positive constant $\sigma > 0$, such that

$$|\dot{d}| \le \frac{\sigma}{2} = \sigma|\phi_2|. \tag{46}$$

In [41], to deal with (46), it set $\dot{d} = \overline{\kappa}\phi_2$ with $|\overline{\kappa}| \le \sigma$. However, as we know, $\dot{d}$ is a variable, which means $\overline{\kappa}$ should not be a constant. However, $\overline{\kappa}$ frequently appears in the derivations of [41], which will cause many difficulties in algebraic manipulations.

Unlike the way in [41], the ingenious way here is that we get the following inequality by combining (44) with (46):

$$|\tilde{g}| = |2\dot{d}| \cdot |\phi_1| \le \sigma|\phi_1| = \sigma|\xi_1|. \tag{47}$$

Then we define

$$\begin{aligned}\omega(\boldsymbol{\xi}, \tilde{g}) &= \sigma^2 {\xi_1}^T \xi_1 - \tilde{g}^2 \\ &= \begin{bmatrix} \boldsymbol{\xi} \\ \tilde{g} \end{bmatrix}^T \begin{bmatrix} \mathbf{R} & 0 \\ 0 & -1 \end{bmatrix} \begin{bmatrix} \boldsymbol{\xi} \\ \tilde{g} \end{bmatrix} \ge 0, \mathbf{R} = \begin{bmatrix} \sigma^2 & 0 \\ 0 & 0 \end{bmatrix}.\end{aligned} \tag{48}$$

To analyze the stability of the system (44), define

$$\begin{cases} V_1 = \boldsymbol{\xi}^T\mathbf{P}\boldsymbol{\xi}, \\ V_2 = 0.5\left(\tilde{k}_1^2 + \tilde{k}_2^2\right), \end{cases} \tag{49}$$

where $\mathbf{P}$ is a positive definite symmetric matrix and the quadratic form $V_1 = \xi^{\mathrm{T}}\mathbf{P}\xi$ is positive definite and radically unbounded by the standard inequality for quadratic forms:

$$\frac{{V_1}^{1/2}(x)}{\lambda_{\max}^{1/2}\{\mathbf{P}\}} \le \|\boldsymbol{\xi}\|_2 \le \frac{{V_1}^{1/2}(x)}{\lambda_{\min}^{1/2}\{\mathbf{P}\}}, \tag{50}$$

where $\|\xi\|_2$ is the Euclidean norm of ξ.

Consider the Lyapunov function candidate

$$V = V_1 + V_2. \tag{51}$$

The positive definite symmetric matrix $\mathbf{P}$ is chosen as follows:

$$\mathbf{P} = \begin{bmatrix} \beta + 4\delta^2 & -2\delta \\ -2\delta & 1 \end{bmatrix}, \tag{52}$$

where $\beta > 0$, then V is continuously derivable except the equilibrium. If the following conditions are satisfied:

$$\begin{cases} 0 < \sigma < 4\delta - 1, \\ k_1 > \dfrac{\left(4\delta^2 - 2\delta + \beta\right)^2}{2\beta(4\delta - \sigma - 1)} + \dfrac{4\delta^2 + \sigma^2 + \sigma}{2\beta}, \end{cases} \tag{53}$$

then the matrix Q defined as (54) is negative definite.

$$\begin{aligned}\mathbf{Q} &= \mathbf{A}^T\mathbf{P} + \mathbf{P}\mathbf{A} + \mathbf{R} + \sigma\mathbf{I} + \mathbf{P}\mathbf{B}\mathbf{B}^{\mathbf{T}}\mathbf{P} \\ &= -\begin{bmatrix} 2k_1\beta - 4\delta^2 - \sigma^2 - \sigma & * \\ -\left(\beta + 4\delta^2\right) + 2\delta & 4\delta - \sigma - 1 \end{bmatrix} < 0,\end{aligned} \tag{54}$$

where $*$ is used to indicate a symmetric element. This conclusion can be easily deduced from (53) and (54) with the Schur complement.

Using (50), the fact can be easily noted that

$$|s|^{1/2} = |\xi_1| \le \|\boldsymbol{\xi}\|_2. \tag{55}$$

Case a. If the adaptive gain k_1 meets condition (53), then substituting (44), (48), and (54) into (49) yields

$$\begin{aligned}\dot{V}_1 &= \dot{\boldsymbol{\xi}}^T\mathbf{P}\boldsymbol{\xi} + \boldsymbol{\xi}^T\mathbf{P}\dot{\boldsymbol{\xi}}\\ &= \dot{\phi}_1\left[\boldsymbol{\xi}^T\left(\mathbf{A}^T\mathbf{P} + \mathbf{P}\mathbf{A}\right)\boldsymbol{\xi} + \tilde{g}\mathbf{B}^T\mathbf{P}\boldsymbol{\xi} + \boldsymbol{\xi}^T\mathbf{P}\mathbf{B}\tilde{g}\right]\\ &= \dot{\phi}_1\begin{bmatrix}\boldsymbol{\xi}\\ \tilde{g}\end{bmatrix}^T\begin{bmatrix}\mathbf{A}^T\mathbf{P} + \mathbf{P}\mathbf{A} & \mathbf{P}\mathbf{B}\\ \mathbf{B}^T\mathbf{P} & 0\end{bmatrix}\begin{bmatrix}\boldsymbol{\xi}\\ \tilde{g}\end{bmatrix} \le \dot{\phi}_1\left\{\begin{bmatrix}\boldsymbol{\xi}\\ \tilde{g}\end{bmatrix}^T\begin{bmatrix}\mathbf{A}^T\mathbf{P} + \mathbf{P}\mathbf{A} & \mathbf{P}\mathbf{B}\\ \mathbf{B}^T\mathbf{P} & 0\end{bmatrix}\begin{bmatrix}\boldsymbol{\xi}\\ \tilde{g}\end{bmatrix} + \omega(\boldsymbol{\xi}, \tilde{g})\right\}\\ &= \dot{\phi}_1\begin{bmatrix}\boldsymbol{\xi}\\ \tilde{g}\end{bmatrix}^T\begin{bmatrix}\mathbf{A}^T\mathbf{P} + \mathbf{P}\mathbf{A} + \mathbf{R} & \mathbf{P}\mathbf{B}\\ \mathbf{B}^T\mathbf{P} & -1\end{bmatrix}\begin{bmatrix}\boldsymbol{\xi}\\ \tilde{g}\end{bmatrix} < \dot{\phi}_1\begin{bmatrix}\boldsymbol{\xi}\\ \tilde{g}\end{bmatrix}^T\begin{bmatrix}-\sigma\mathbf{I} & 0\\ 0 & 0\end{bmatrix}\begin{bmatrix}\boldsymbol{\xi}\\ \tilde{g}\end{bmatrix}\\ &= -\dot{\phi}_1\sigma\boldsymbol{\xi}^T\boldsymbol{\xi}\\ &= -\frac{|s|^{-1/2}\sigma\boldsymbol{\xi}^T\boldsymbol{\xi}}{2}.\end{aligned} \tag{56}$$

Combing (50) and (55), (56) can be written as

$$\dot{V}_1 \le -\mu {V_1}^{1/2}, \tag{57}$$

where μ is

$$\mu = \frac{\sigma\lambda_{\min}^{1/2}\{\mathbf{P}\}}{2\lambda_{\max}\{\mathbf{P}\}}. \tag{58}$$

Substituting (32) and (33) into (49) yields

$$\begin{aligned}\dot{V}_2 &= \tilde{k}_1\dot{k}_1 + \tilde{k}_2\dot{k}_2\\ &= -\eta\left(|\tilde{k}_1| + |\tilde{k}_2|\right) - \lambda|\tilde{k}_1||s|^{\alpha} - 2\delta\lambda|\tilde{k}_2||s|^{\alpha} + \eta\left(|\tilde{k}_1| + |\tilde{k}_2|\right)\\ &\le -\eta\left(|\tilde{k}_1| + |\tilde{k}_2|\right) - (\lambda|s|^{\alpha} - \eta)|\tilde{k}_1| - |\tilde{k}_2|(2\lambda\delta|s|^{\alpha} - \eta),\end{aligned} \tag{59}$$

where $\eta > 0$. Noting $(|\tilde{k}_1| + |\tilde{k}_2|)^2 \ge \tilde{k}_1^2 + \tilde{k}_2^2$, if $|s| > \varepsilon$, $k_1 > k_m$ and that

$$|s| > \varphi = \max\left\{\left(\frac{\eta}{\lambda}\right)^{1/\alpha}, \left(\frac{\eta}{2\lambda\delta}\right)^{1/\alpha}\right\}. \tag{60}$$

one can imply that

$$\dot{V}_2 \le -\eta\left(|\tilde{k}_1| + |\tilde{k}_2|\right) \le -\sqrt{2}\eta V_2^{1/2}. \tag{61}$$

The following inequality is obtained by using (57) and (61):

$$\dot{V} \le -\mu {V_1}^{1/2} - \sqrt{2}\eta V_2^{1/2} \le -\min\{\mu, \sqrt{2}\,\eta\}V^{1/2}. \tag{62}$$

With Lemma 3, it can be concluded that the following region can be reached in finite time:

$$\Omega_1 = \{s \| |s| \le \max\{\varepsilon, \varphi\}\}. \tag{63}$$

If $\varepsilon < |s| < \varphi$, the adaptive gains k_1 and k_2 continue to increase until $|s| < \varepsilon$.

Case b. When the adaptive gain $k_1 < k_m$, k_1 and k_2 starts to increase until $|s| < \varepsilon$, the time derivative of (51) is

$$\dot{V} = \dot{V}_1 + \dot{V}_2 \le -\mu {V_1}^{1/2} - \gamma|\tilde{k}_1||s| - 2\delta\gamma|\tilde{k}_2||s| < 0, \tag{64}$$

which indicates the closed-loop system is uniformly bounded when $k_1 < k_m$.

In summary, the system state s will converge to $|s| < \varepsilon$ within a finite reaching time T_r.

On the sliding surface, it follows from (13) and (30) that

$$\begin{cases}\dot{x}_1 = x_2,\\ \dot{x}_2 = -\sum_{i=1}^{2} c_i\left(1 - e^{-t/\tau_i}\right)|x_i|^{\alpha_i}\operatorname{sign}(x_i).\end{cases} \tag{65}$$

Here, we introduce the vector field h: $\mathbb{R}^2 \longrightarrow \mathbb{R}^2$

$$\begin{aligned}h(x_1, x_2) &= [h_1, h_2]^T\\ &= [\dot{x}_1, \dot{x}_2]^T.\end{aligned} \tag{66}$$

The trajectories of function (66) are invariant with respect to the transformation

$$\forall\eta > 0, H_\eta\colon\ (x_1, x_2) \mapsto \left(\eta^{2-\alpha_2}x_1, \eta x_2\right). \tag{67}$$

From (65)–(67) and $\alpha_1 = \alpha_2/(2 - \alpha_2)$, we can get

$$\begin{cases}h_1\left(\eta^{2-\alpha_2}x_1, \eta x_2\right) = \eta^{(2-\alpha_2)+(\alpha_2-1)}h_1(x_1, x_2),\\ h_2\left(\eta^{2-\alpha_2}x_1, \eta x_2\right) = \eta^{1+(\alpha_2-1)}h_2(x_1, x_2),\end{cases} \tag{68}$$

which shows the system (66) is homogeneous of degree $\alpha_2 - 1 < 0$ with respect to dilation $(2 - \alpha_2, 1)$. With Lemma 1 in mind, system (65) is finite-time stable. Therefore, the tracking errors, x_1 and x_2, converge to a small region near zero on the sliding surface within a finite time T_s.

Since the reaching time T_r and the sliding time T_s are both finite, the tracking errors of LOS angle x_1 and LOS angular rate x_2 will converge to a small region near zero within a finite time $T = T_r + T_s$.

5. Simulation Results

In this section, some numerical simulations are performed to illustrate the performance of the proposed composite guidance law, TD and DO. The simulations are performed using the implicit Euler discretization with a fixed step size of 0.01 s for updating the system states. Suppose the range r, LOS angle q, and noisy target heading angle $\widetilde{\theta}_T$ can be provided by the electric-field detection device.

The target is a kind of large warship with a turning angular rate less than $2^\circ/s$. It should be pointed out that the interception with an impact angle can only be realized under some initial conditions of engagement. Moreover, large initial heading errors may result in a target missed or a predetermined impact angle not being obtained. This conclusion is consistent with practical application, for the fact mentioned above in the introduction that the SCT has limited maneuverability to maintain super-cavity stability. To achieve the desired impact angle, the torpedo launch platform needs to change the initial engagement by prelaunch maneuver.

For brevity, only one kind of typical initial engagement condition is considered here. In the inertial coordinate system, the initial positions of the torpedo and the target are $(0, 0)$ and (960, 720), with the initial relative range $r(0) = 1200\,m$. The constant velocities for the torpedo and the target are $V_M = 100$ m/s and $V_T = 15$ m/s. The initial heading angles of the torpedo and the target are $\theta_M(0) = 10^\circ$ and $\theta_T(0) = 0^\circ$. The limited maneuverability of a torpedo can be described by $\dot{\theta}_M \le 12^\circ$ or $a_M \le 21\text{m/s}^2$.

Two intercepting scenarios with different escaping maneuvers are considered. In Case 1, the target is executing a constant maneuver. In Case 2, the target is assumed to execute a sinusoidal maneuver [42]. Several critical parameters need to be tuned, and the regulating rules of these parameters are discussed under each component's description. Simulation parameters for the proposed guidance law are listed in Table 1.

Additionally, the positive coefficients λ_{1i}, λ_{2i}, and λ_{3i} can be set following the recursive sequences in [26], which are partly listed in Table 2.

Table 1: Simulation parameters in guidance law.

Parameters	Belongs to	Case 1	Case 2
L_1	TD1	0.01	0.01
χ	TD2	600	600
κ	TD2	2	2
τ_0	TD2	0.5 s	0.5 s
β	TD2	0.5	0.5
L_2	DO1	0.6	1.2
c_1	NNTSM	0.05	0.045
τ	Autopilot	0.05 s	0.05 s
c_2	NNTSM	0.15	0.15
τ_1, τ_2	NNTSM	1.6 s	1.6 s
γ	ASTA	5	5
λ	ASTA	1	1
k_m	ASTA	0.15	0.15
ε	ASTA	0.1	0.1
δ	ASTA	0.05	0.05

Table 2: Recursive sequences of 1st order and 3rd order.

Order	λ_0	λ_1	λ_2	λ_3	Component
1st order	1.1	1.5			
2nd order	1.1	2.12	2		λ_{2i} in DO1, λ_{3i} in TD2
3rd order	1.1	3.06	4.16	3	λ_{1i} in TD1

Case 1. Constant Maneuvering Targets

According to the actual maneuverability of the target warship, we assume that the target is executing counterclockwise rotation maneuvers with an angular rate of $\omega = 0.04$rad/s.

The impact angle constraint for SCT is not for a "hit to kill" interception to improve warhead effectiveness [14, 18] but for making use of the target scale to increase hit probability, given that a larger impact angle corresponds to a larger interception width. Simulations are performed with two different desired impact angles, -25° and -45°, and the results are shown in Figure 4.

The interception geometries are shown in Figure 4(a). Under the control law (37), the interceptions of a constant maneuvering target at different impact angles, -25° and -45°, can be achieved. Different corresponding lateral acceleration profiles are shown in Figure 4(b), indicating that the impact angle of -45° requires a larger magnitude of acceleration. That is the fact that with different desired impact angles, various tracking errors are to be eliminated, and a more significant initial LOS angle error demands a more considerable acceleration. As shown in Figures 4(c) and 4(d), both the LOS angle error x_1 and the LOS angular rate error x_2 converge to zero in finite time, and larger initial errors bring about longer convergence time. In addition, the interception with the impact angle of -45°, of which the initial tracking errors are more prominent, takes a little more attacking time.

As shown in Figure 4(e), the TD-N (TD2) for processing the virtual control command x_{3c} is compared with traditional TDs, with the impact angle selected as -45°. The TD-N can acquire the best tracking result, while a time delay can be found in the tracking responses of both TD-L and TD-H during the initial transient. This deficiency will bring about the reduction of control accuracy in the design of autopilot control input, as discussed in part C of Section 5.

The proposed DO1 is compared with ESO reported in [22] under the impact angle of -45°. From Figure 4(f), the two disturbance observers can all estimate the a_{Tq} precisely after an initial transient period. The transient time of proposed DO1 is approximately the same as that of ESO. However, the estimation result via ESO has a larger overshoot, which is undesirable and may bring about the saturation of autopilot control input. What's more, there are several parameters that need to be prudently tuned in ESO [45], making it more difficult in application.

Case 2. Weaving Maneuver Target

It is assumed that the target weaving acceleration is chosen as $a_{Tq} = 0.6 \sin(\pi t/10)\text{m/s}^2$.

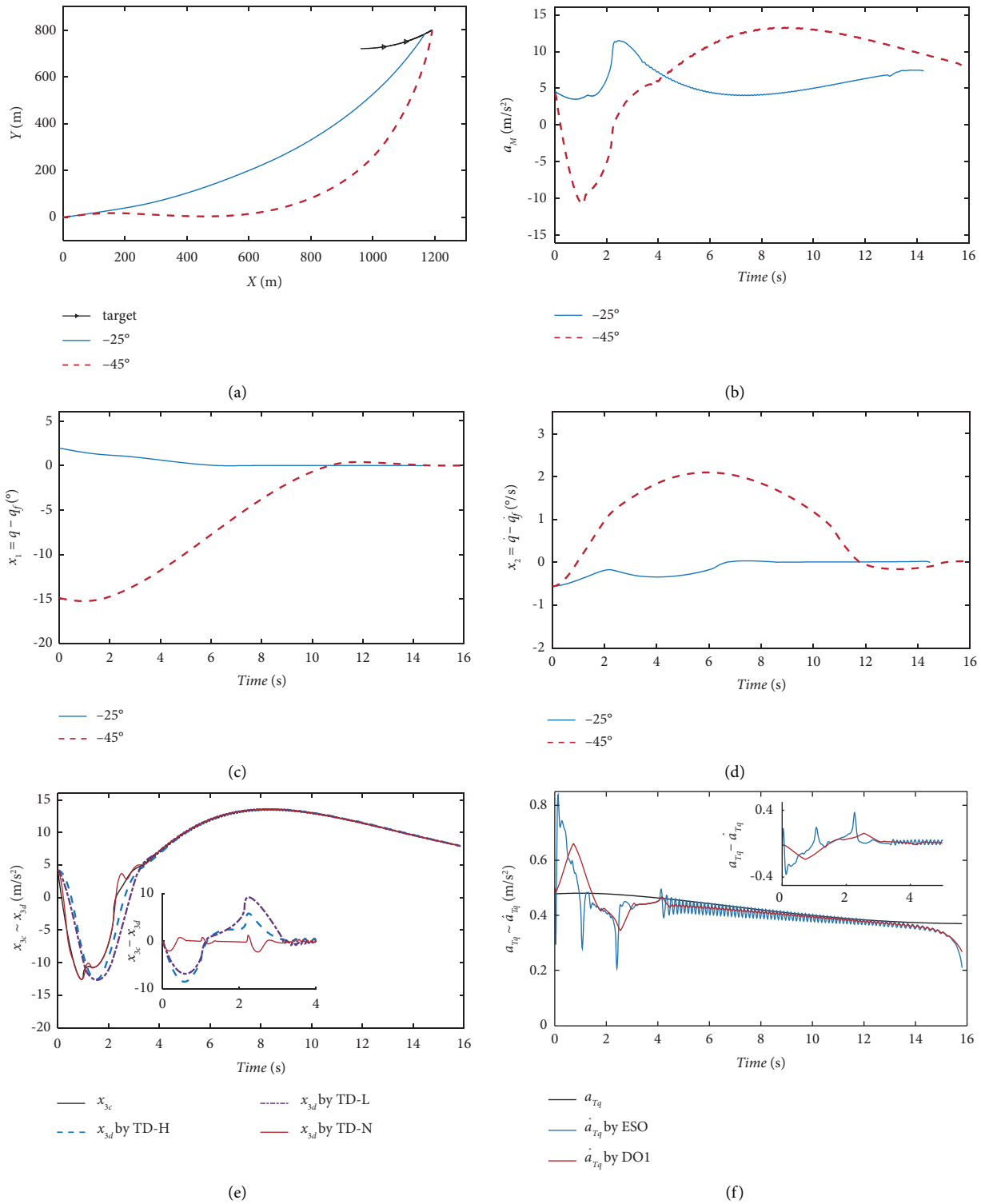

FIGURE 4: Simulation results in Case 1. (a) Interception trajectories. (b) Acceleration profiles of torpedo. (c) LOS angle error. (d) LOS angular rate error. (e) Tracking of the virtual control command. (f) Estimate of target lateral acceleration.

The traditional discontinuous sliding mode control guidance law (TDSMG) and the super-twisting sliding mode control guidance law (STSMG) are also performed in the simulation for comparison.

In TDSMG, the adaptive super-twisting algorithm is substituted by the reaching law of constant plus proportional rate strategy, while the same DO1 for estimating target lateral acceleration and the same TD2 for processing the

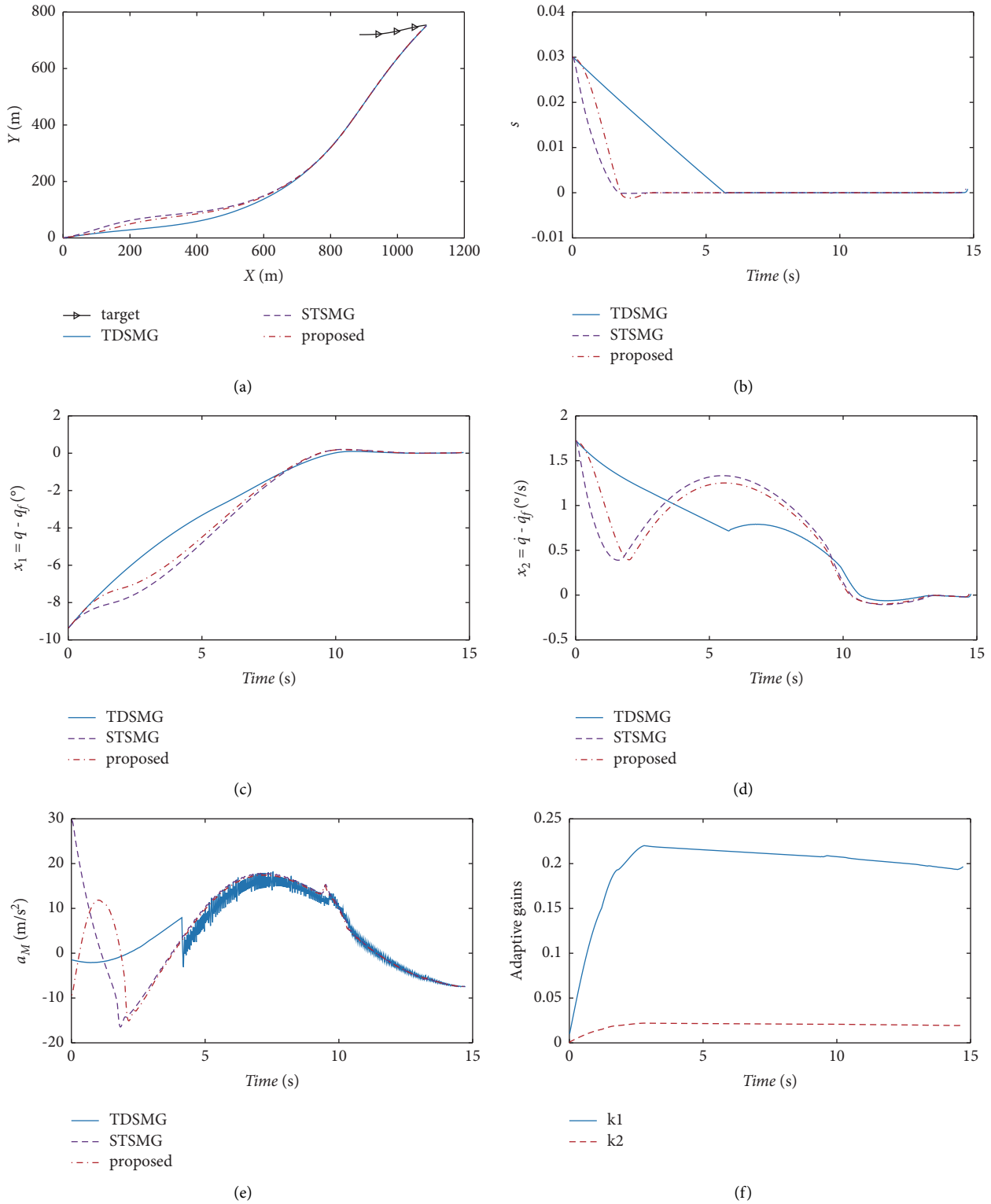

FIGURE 5: Simulation results in Case 2. (a) Trajectories of target and torpedo. (b) Occurrence of sliding mode. (c) LOS angle error. (d) LOS angular rate error. (e) Acceleration of torpedo. (f) Change of adaptive gains.

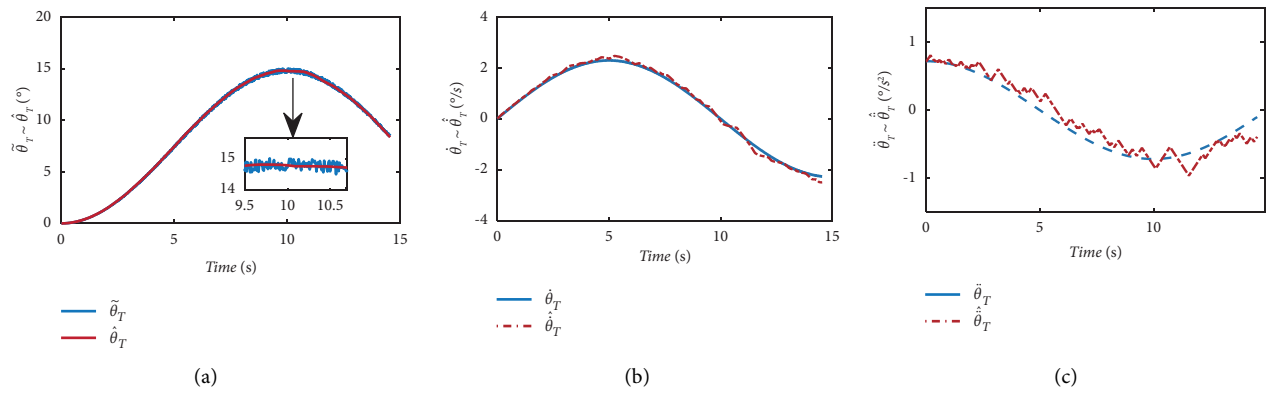

FIGURE 6: Output of TD1 with the noisy heading angle of the target. (a) Target heading angle with noise and its reconstruction. (b) 1st-order derivative estimate of target heading angle. (c) 2nd-order derivative estimate of target heading angle.

virtual control command are still adopted. As a result, the virtual control command changes into

$$x_{3c}' = \frac{r}{\cos\eta_M}\left[\sum_{i=1}^{2} c_i\left(1-e^{-t/\tau_i}\right)|x_i|^{\alpha_i}\operatorname{sign}(x_i) - \hat{\dot{\theta}}_T - \frac{2\dot{r}\dot{q}}{r} + \frac{\hat{a}_{Tq}}{r} + k_3 s + k_4\cdot\operatorname{sign}(s)\right]. \tag{69}$$

In STSMG, the standard super-twisting algorithm and nonlinear integral sliding manifold in [21] are employed, with the virtual control command chosen as

$$x_{3c}'' = \frac{r}{\cos\eta_M}\left[\sum_{i=1}^{2} c_i|x_i|^{\alpha_i}\operatorname{sign}(x_i) - \hat{\ddot{\theta}}_T - \frac{2\dot{r}\dot{q}}{r} + \frac{\hat{a}_{Tq}}{r} + k_5\phi_1 + \int k_6\phi_2 dt\right]. \tag{70}$$

Here, we set the fixed parameters $k_5 = 0.2$ and $k_6 = 0.01$ with the assumption of known upper bounds of d and $\dot{d}$.

The simulation results are shown in Figure 5, with the desired impact angle selected as -40°. Figure 5(a) shows that the torpedo hits the target with desired impact angle under different guidance laws. All three guidance laws can ensure a finite-time convergence of the sliding variable in reaching phase, which is shown in Figure 5(b). It can be inferred from Figures 5(c) and 5(d) that, similar to Case 1, the LOS angle error x_1 and the LOS angular rate error x_2 converge to zero in finite time. As can be seen from Figure 5(e), compared with TDSMG, the proposed guidance law and STSMG can eliminate the chattering caused by discontinuous terms in the sliding phase. Furthermore, compared with STSMG, the proposed guidance law can avoid the undesirable extremely large acceleration at the initial time, which is beyond the maneuverability limit of the SCT. By comparing the virtual control command (34) and (70), one can observe that x_{3c} is attenuated due to $1 - e^{-t/\tau_i} < 1$ and small adaptive gains k_1, k_2 at the beginning. Figure 5(f) shows the variation profiles of adaptive gains k_1, k_2, which gradually increase in the reaching phase and decrease in the sliding phase.

The performance of TD1, which is used to process the measured heading angle of the target, is evaluated under the following noisy measurement signal:

$$\tilde{\theta}_T = \theta_T + 0.03\delta, \tag{71}$$

where $\delta \sim N(0,1)$ is the unit Gaussian white noise. On the one hand, the TD1 acts as a filter, reconstructing a noiseless signal from the measurement signal, as shown in Figure 6(a). On the other hand, the TD1 works as a differentiator, acquiring the first-order and second-order derivatives of the measurement signal. As shown in Figures 6(b) and 6(c), the estimations are close to the theoretical ones, which meets the need for exact θ_T, $\dot{\theta}_T$, and the unknown external disturbance $\ddot{\theta}_T$.

6. Conclusions

Provided suitable parameters choice, the high-order sliding mode TD1 has a good denoising effect on the measurement signal $\tilde{\theta}_T$, which meets the need for exact θ_T, $\dot{\theta}_T$, and $\ddot{\theta}_T$. The novel DO1 proposed in this article improves the estimation of target lateral acceleration in real time. With the help of TD1 and the proposed DO1, the problem of insufficient target maneuver information in guidance law design is solved. A novel composite guidance law with finite-time

convergence and impact angle constraint is presented based on a new nonsingular terminal sliding manifold and adaptive super-twisting algorithm. A new TD2 is applied for dynamic surface control, replacing the first-order integral filter, and high-accuracy tracking of the virtual control command can be realized.

Simulation results verify that, under the proposed guidance law, an SCT can achieve interception with predetermined impact angle constraints under suitable initial conditions, ensuring the LOS angle error and the LOS angular rate error converge to zero in finite time. In addition, utilizing the revised sliding manifold and the adaptive super-twisting algorithm, the control input of autopilot is significantly reduced, and the chattering phenomenon is eliminated, making it more suitable for practical applications.

One shortcoming of the proposed guidance law is that there is a short time for the TDs and DO to be stable, which makes it disabled when the target is found at a too-close distance and the time for interception is extremely short. Therefore, a larger detection range of SCT, which is becoming a reality with the development of electric-field detection technology, will benefit its performance at the terminal phase. Moreover, the capture region of the proposed guidance law, which refers to the initial engagement conditions that make the interception occur, has yet to be studied. Only with a known capture region can the launch platform occupy a favorable position by prelaunch maneuver. Thus, a theoretical analysis should be made on the initial conditions for better application of the new guidance law in future research.

Data Availability

The data used to support the findings of this study are available from the corresponding author upon request.

Conflicts of Interest

The authors declare that there are no conflicts of interest regarding the publication of this paper.

Acknowledgments

This paper was supported in part by the National Natural Science Foundation of China (nos. 62073334 and 62101579).

References

[1] P. Yu, J. Cheng, and J. Zhang, "Ship target tracking using underwater electric field," *Progress In Electromagnetics Research M*, vol. 86, pp. 49–57, 2019.

[2] J. Zhang, P. Yu, R. Jiang, and X. Tao-tao, "Real-time Localization for Underwater Equipment Using an Extremely Low Frequency Electric Field," *Defence Technology*, 2022.

[3] Y. N. Savchenko, V. N. Semenenko, and G. Y. Savchenko, "Peculiarities of supercavitating vehicle's maneuvering," *International Journal of Fluid Mechanics Research*, vol. 46, no. 4, pp. 309–323, 2019.

[4] P. Lu, D. B. Doman, and J. D. Schierman, "Adaptive terminal guidance for hypervelocity impact in specified direction," *Journal of Guidance, Control, and Dynamics*, vol. 29, no. 2, pp. 269–278, 2006.

[5] T.-H. Kim, B.-G. Park, and M.-J. Tahk, "Bias-shaping method for biased proportional navigation with terminal-angle constraint," *Journal of Guidance, Control, and Dynamics*, vol. 36, no. 6, pp. 1810–1816, 2013.

[6] A. Ratnoo and D. Ghose, "Impact angle constrained guidance against nonstationary nonmaneuvering targets," *Journal of Guidance, Control, and Dynamics*, vol. 33, no. 1, pp. 269–275, 2010.

[7] B. S. Kim, J. G. Lee, and H. S. Han, "Biased PNG law for impact with angular constraint," *IEEE Transactions on Aerospace and Electronic Systems*, vol. 34, no. 1, pp. 277–288, 1998.

[8] C. K. Ryoo, H. Cho, and M. J. Tahk, "Time-to-go weighted optimal guidance with impact angle constraints," *IEEE Transactions on Control Systems Technology*, vol. 14, no. 3, pp. 483–492, 2006.

[9] V. Shaferman and T. Shima, "Linear quadratic guidance laws for imposing a terminal intercept angle," *Journal of Guidance, Control, and Dynamics*, vol. 31, no. 5, pp. 1400–1412, 2008.

[10] Y.-I. Lee, S.-H. Kim, and M.-J. Tahk, "Analytic solutions of optimal angularly constrained guidance for first-order lag system," *Proceedings of the Institution of Mechanical Engineers - Part G: Journal of Aerospace Engineering*, vol. 227, no. 5, pp. 827–837, 2013.

[11] D. Cho, H. J. Kim, and M. J. Tahk, "Impact angle constrained sliding mode guidance against maneuvering target with unknown acceleration," *IEEE Transactions on Aerospace and Electronic Systems*, vol. 51, no. 2, pp. 1310–1323, 2015.

[12] D. Zhou, P. Qu, and S. Sun, "A guidance law with terminal impact angle constraint accounting for missile autopilot," *Journal of Dynamic Systems, Measurement, and Control*, vol. 135, no. 5, 2013.

[13] G. Marks, Y. Shtessel, H. Gratt, and S. Ilya, "Effects of high order sliding mode guidance and observers on hit-to-kill interceptions," in *AIAA Guidance, Navigation, and Control Conference and Exhibit*, G. Marks, Y. Shtessel, H. Gratt, and I. Shkolnikov, Eds., p. 5967, American Institute of Aeronautics and Astronautics, Reston, Virigina, 2005.

[14] Y. B. Shtessel, I. A. Shkolnikov, and A. Levant, "Guidance and control of missile interceptor using second-order sliding modes," *IEEE Transactions on Aerospace and Electronic Systems*, vol. 45, no. 1, pp. 110–124, 2009.

[15] Z. Zhang, S. Li, and S. Luo, "Composite guidance laws based on sliding mode control with impact angle constraint and autopilot lag," *Transactions of the Institute of Measurement and Control*, vol. 35, no. 6, pp. 764–776, 2013.

[16] S. R. Kumar, S. Rao, and D. Ghose, "Sliding-mode guidance and control for all-aspect interceptors with terminal angle constraints," *Journal of Guidance, Control, and Dynamics*, vol. 35, no. 4, pp. 1230–1246, 2012.

[17] S. MengXiuyun and Q. Song, "Design and simulation of guidance law with angular constraint based on non-singular terminal sliding mode," *Physics Procedia*, vol. 25, pp. 1197–1204, 2012.

[18] S. R. Kumar, S. Rao, and D. Ghose, "Nonsingular terminal sliding mode guidance with impact angle constraints," *Journal of Guidance, Control, and Dynamics*, vol. 37, no. 4, pp. 1114–1130, 2014.

[19] Y. Feng, X. Yu, and Z. Man, "Non-singular terminal sliding mode control of rigid manipulators," *Automatica*, vol. 38, no. 12, pp. 2159–2167, 2002.

[20] L. Yang and J. Yang, "Nonsingular fast terminal sliding-mode control for nonlinear dynamical systems," *International Journal of Robust and Nonlinear Control*, vol. 21, no. 16, pp. 1865–1879, 2011.

[21] Z. Zhang, S. Li, and S. Luo, "Terminal guidance laws of missile based on ISMC and NDOB with impact angle constraint," *Aerospace Science and Technology*, vol. 31, no. 1, pp. 30–41, 2013.

[22] J. Han, "From PID to active disturbance rejection control," *IEEE Transactions on Industrial Electronics*, vol. 56, no. 3, pp. 900–906, 2009.

[23] B. Z. Guo and Z. L. Zhao, "On convergence of tracking differentiator," *International Journal of Control*, vol. 84, no. 4, pp. 693–701, 2011.

[24] J. Zhang, X. Shao, W. Zhang, and J. Na, "Pathh of reinforcing transient performances for networked mobile robots over a single curve," *IEEE Transactions on Instrumentation and Measurement*, vol. 34, no. 3, pp. 379–384, 1998.

[25] A. Levant, "Robust exact differentiation via sliding mode technique," *Automatica*, vol. 34, no. 3, pp. 379–384, 1998.

[26] A. Levant, "Higher-order sliding modes, differentiation and output-feedback control," *International Journal of Control*, vol. 76, no. 9-10, pp. 924–941, 2003.

[27] A. Levant and M. Livne, "Robust exact filtering differentiators," *European Journal of Control*, vol. 55, pp. 33–44, 2020.

[28] J. Yu, S. Jin, X. Wang, X. Xiong, Z. Lv, and Y. Jin, "A variable gain sliding mode tracking differentiator for derivative estimation of noisy signals," *IEEE Access*, vol. 8, Article ID 148500, 2020.

[29] D. Zhou, S. Sun, and K. L. Teo, "Guidance laws with finite time convergence," *Journal of Guidance, Control, and Dynamics*, vol. 32, no. 6, pp. 1838–1846, 2009.

[30] D. Swaroop, J. K. Hedrick, P. P. Yip, and J. Gerdes, "Dynamic surface control for a class of nonlinear systems," *IEEE Transactions on Automatic Control*, vol. 45, no. 10, pp. 1893–1899, 2000.

[31] L. Wang, W. Zhang, D. Wang, K. Peng, and H. Yang, "Command filtered back-stepping missile integrated guidance and autopilot based on extended state observer," *Advances in Mechanical Engineering*, vol. 9, no. 11, Article ID 168781401773325, 2017.

[32] T. Ju, J. Yu, C. Ming, X. Wang, and X. Gu, "Three-dimensional integrated guidance and control for a STT missile based on improved RISE in series," *IEEE Access*, vol. 7, Article ID 137887, 2019.

[33] Z. Zhu, D. Xu, J. Liu, and Y. Xia, "Missile guidance law based on extended state observer," *IEEE Transactions on Industrial Electronics*, vol. 60, no. 12, pp. 5882–5891, 2013.

[34] S. P. Bhat and D. S. Bernstein, "Geometric homogeneity with applications to finite-time stability," *Mathematics of Control, Signals and Systems*, vol. 17, no. 2, pp. 101–127, 2005.

[35] A. Levant and X. Yu, "Sliding-mode-based differentiation and filtering," *IEEE Transactions on Automatic Control*, vol. 63, no. 9, pp. 3061–3067, 2018.

[36] A. Levant and M. Livne, "Weighted homogeneity and robustness of sliding mode control," *Automatica*, vol. 72, pp. 186–193, 2016.

[37] S. He and D. Lin, "Guidance laws based on model predictive control and target manoeuvre estimator," *Transactions of the Institute of Measurement and Control*, vol. 38, no. 12, pp. 1509–1519, 2016.

[38] X. Shao, J. Zhang, L. Xu, and W. Zhang, "Appointed-time Guaranteed Adaptive Fault-Tolerant Attitude Tracking for Quadrotors with Aperiodic Data Updating," *Aerospace Science and Technology*, Article ID 107881, 2022.

[39] E. Bernuau, D. Efimov, W. Perruquetti, and A. Polyakov, "On homogeneity and its application in sliding mode control," *Journal of the Franklin Institute*, vol. 351, no. 4, pp. 1866–1901, 2014.

[40] Y. Shtessel, M. Taleb, and F. Plestan, "A novel adaptive-gain supertwisting sliding mode controller: methodology and application," *Automatica*, vol. 48, no. 5, pp. 759–769, 2012.

[41] S. He and D. Lin, "Observer-based guidance law against maneuvering targets without line-of-sight angular rate information," *Proceedings of the Institution of Mechanical Engineers - Part G: Journal of Aerospace Engineering*, vol. 230, no. 10, pp. 1827–1839, 2016.

[42] F. Plestan, Y. Shtessel, V. Bregeault, and A. Poznyak, "New methodologies for adaptive sliding mode control," *International Journal of Control*, vol. 83, no. 9, pp. 1907–1919, 2010.

[43] J. A. Moreno, "A linear framework for the robust stability analysis of a generalized super-twisting algorithm," in *Proceedings of the 2009 6th International Conference on Electrical Engineering, Computing Science and Automatic Control (CCE)*, pp. 1–6, IEEE, Toluca, Mexico, January 2009.

[44] J. A. Moreno and M. Osorio, "Strict Lyapunov functions for the super-twisting algorithm," *IEEE Transactions on Automatic Control*, vol. 57, no. 4, pp. 1035–1040, 2012.

[45] W. Zhang, X. Shao, W. Zhang, J. Qi, and H. Li, "Unknown Input Observer-Based Appointed-Time Funnel Control for Quadrotors," *Aerospace Science and Technology*, vol. 126, Article ID 107351, 2022.